Stimulating Lewis Acid of Pt-O-Co Bridge via Vacancy Engineering for Efficient Hydrogen Evolution in Seawater

Mengyue Gao [a], Junfeng Qin [b*], Rui Zhang [a,c], Xu Liu [a,c], Yuxin Liu [a,c], Yuxin Zhang [a,c], Long Song [a], Jingyi Xie [d], Jingqi Chi [a*], Xiaobin Liu [a,c*], Lei Wang [a*]

a Key Laboratory of Eco-chemical Engineering, International Science and Technology Cooperation Base of Eco-chemical Engineering and Green Manufacturing, College of Chemical Engineering, Qingdao University of Science and Technology, Qingdao 266042, PR China

b Hunan Provincial Key Laboratory of Water Treatment Functional Materials, College of Chemistry and Materials Engineering, Hunan University of Arts and Science, Changde 415000, Hunan, People's Republic of China

c College of Environment and Safety Engineering, Qingdao University of Science and Technology, Qingdao 266042, PR China

d Key Laboratory of materials and surface technology (Ministry of Education), School of Materials Science and Engineering, Xihua University, Chengdu, 610039, China

E-mail: qinjunfeng@huas.edu.cn, chijingqi@qust.edu.cn, liuxb@qust.edu.cn, inorchemwl@126.com

1. Experimental Section

1.1. Materials and Chemicals

The reagents used in this work included nickel foam (NF), hydrochloric acid, acetone, ethanol, deionized water, cobalt(II) nitrate hexahydrate ($Co(NO_3)_2·6H_2O$), urea ($CO(NH_2)_2$), ammonium fluoride (NH_4F), sodium borohydride ($NaBH_4$), chloroplatinic acid hexahydrate ($H_2PtCl_6·6H_2O$), sodium thiosulfate ($Na_2S_2O_3$), potassium hydroxide (KOH), and sodium chloride (NaCl). The seawater utilized for the experiments was collected from the Shilaoren Bathing Area in Qingdao, Shandong Province.

1.2. Materials Synthesis

1.2.1. Synthesis of CoO Precursors

To fabricate the CoO precursor, a 1.0 × 2.0 cm^2 piece of nickel foam was ultrasonically cleaned for 20 min in 0.1 M HCl, acetone, and ethanol successively to

remove surface oxides and organic impurities. The pretreated NF was then immersed in 30 mL of deionized water containing NH_4F, $CO(NH_2)_2$, and $Co(NO_3)_2·6H_2O$. The solution was sealed in a stainless-steel autoclave and maintained at 120 °C for 9 h. After naturally cooling to room temperature, the resulting product was rinsed several times with ethanol and deionized water, followed by drying to obtain the CoO precursor.

1.2.2. Synthesis of CoO_x

The as-prepared CoO precursor was soaked in 25 mL of aqueous solution containing 0.15 g $NaBH_4$ at room temperature for 30 min. After drying, the reduced product was denoted as CoO_x.

1.2.3. Synthesis of Pt-CoO_x

To load Pt species, the CoO_x sample was immersed in 10 mL of solution containing 36 mg $H_2PtCl_6·6H_2O$ and kept at room temperature for 1 h. The product was then dried to yield Pt-CoO_x.

1.2.4. Synthesis of S-(Ni,Fe)OOH

The porous S-(Ni,Fe)OOH catalyst was prepared via a one-step, room-temperature solution-phase method on a nickel foam substrate. Briefly, 0.35 g $Fe(NO_3)_3·9H_2O$ and 0.05 g $Na_2S_2O_3·5H_2O$ were dissolved in 10 mL of deionized water, after which a 1 × 2 cm^2 piece of commercial nickel foam was immersed in the solution for 5 min to complete the synthesis.[1]

1.2.5. Synthesis of Pt/C

First, 460 μL of anhydrous ethanol was mixed with 40 μL of naphthol to form a homogeneous solution. Then, 5 mg of Pt/C was added, and the mixture was ultrasonicated for 30 minutes to prepare the catalyst ink. The resulting ink was uniformly dropped onto a clean glass slide and dried under a heat lamp.

1.3. Materials characterization

The crystal structure and composition of the catalysts were analyzed by X-ray diffraction (XRD, X 'PERT PRO MPD) within a 2θ range of 3-90° at a scanning rate of 5° min^{-1}. The morphology and elemental distribution were examined using

scanning electron microscopy (SEM, Hitachi S-8200) and transmission electron microscopy (TEM, JEM-2100UHR) equipped with energy-dispersive X-ray spectroscopy (EDS). The elemental composition was quantitatively determined by inductively coupled plasma mass spectrometry (ICP-MS, Agilent 7850). Surface chemical states and valence information were obtained from X-ray photoelectron spectroscopy (XPS, AXIS SUPRA) employing a monochromatic Al Kα source (15 mA, 14 kV).

1.4. Electrochemical Measurements

Electrochemical tests were carried out on a Gamry Reference 3000 workstation using a standard three-electrode configuration at ambient temperature. A graphite rod (5 mm diameter) was used as the counter electrode, a saturated calomel electrode (SCE) as the reference, and a 1 × 2 cm^2 catalyst-coated nickel foam as the working electrode. All measured potentials were referenced to the reversible hydrogen electrode (RHE) according to the equation: E (RHE) = E (Hg/HgO) + 0.243 V + 0.059 pH. Hydrogen evolution reaction (HER) performance was evaluated in 1.0 M KOH, 1.0 M KOH + 0.5 M NaCl, and 1.0 M KOH + seawater (sw) electrolytes using linear sweep voltammetry (LSV) at a scan rate of 5 mV s^{-1}. All polarization data were corrected for 100% iR compensation. The Tafel slope (b) was derived from the relation $\eta = a + b \log (j)$, where j denotes the current density. The electrochemically active surface area (ECSA) was estimated via cyclic voltammetry (CV) within the non-faradaic region at scan rates ranging from 20 to 100 mV s^{-1}. Catalyst durability was further assessed by chronopotentiometric measurements in 1.0 M KOH + sw electrolyte at room temperature.

1.5. Theoretical calculations

All calculations were performed using the density functional theory (DFT) technique using the Vienna ab initio simulation package (VASP).[2] Spin-polarized calculations were performed using the generalized gradient approximation (GGA) combined with the Perdew-Burke-Ernzerhof (PBE) method to determine the exchange and correlation energies. The projector-augmented wave (PAW) method was used to

represent the core-valence electron interactions. DFT+U correction was used in the calculation process, the correction values for U were as follows: Co 3.5 eV. The typical plane-wave cutoff energy was 400 eV for basis-set expansion. For geometry optimization calculations, forces were converged below 0.03 eV/Å. The SCF convergence energy was 1×10^{-4} eV. A $1 \times 1 \times 1$ k-point mesh was used to perform all the calculations.

Four-layer slab model surfaces of CoO substitutions were built to calculate the adsorption energies and Gibbs free energies. Three p (3×3) unit cell expansions were used to model the surface of CoO(111). One Pt atom was doped into the surface of CoO(111) to construct the Pt-CoO model. And a oxygen vacancy near Pt atom was moved out for simulating Pt-CoO_x model. A vacuum of 15 Å was used to simulate the surface under periodic boundary conditions.

The adsorption energy (E_{ads}) of the OH and the other molecule on the surface was calculated as follows (eq 1):

$$E_{ads} = E_{adsorbate + surface} - E_{surface} - E_{gas}, \quad (1)$$

where $E_{surface}$ is the clean surface relaxation energy of the surface slab, E_{gas} is the energy of a free gas molecule under conditions of vacuum, and $E_{adsorbate + surface}$ is the energy of the composite system.

The barrier energy, ΔE, for a difference between transition state energy difference and standard product formation enthalpy is defined as follows. The energy barrier calculation of H_2O to H-OH on Pt-CoO as an example (eq 2):

$$\Delta E = \left(E_{H-OH-Pt-CoO} - E_{stab-Pt-CoO}\right) - \left(E_{H2O-Pt-CoO} - E_{stab-Pt-CoO}\right) \quad (2)$$

where $E_{H\text{-}OH\text{-}Pt\text{-}CoO}$ and $E_{H2O\text{-}Pt\text{-}CoO}$ are the energies of the H-OH and H_2O adsorbed on Pt-CoO, $E_{stab\text{-}Pt\text{-}CoO}$ is the energy of the Pt-CoO structure surface slab. As the calculations are performed a t =0 K at a fixed cell volume, the differences in the Gibbs free energy should equal the differences in the total energy. By this definition, the lower the ΔE is, the easier it is to react.

1.6. Energy efficiency caclulations

When the typical current density in alkaline water electrolyzers (AWEs) is 0.5 A/cm², the work (W) was calculated using Eq. 1, based on the unit electric quantity (Q) and cell voltage (V). In the standard state, the volume of hydrogen per mole is 22.4×10^{-3} Nm³, allowing Q to be determined using Eq. 2.

$$W=Q\times V/1000 \text{ kW h Nm}^{-3} \quad (1)$$

$$Q=2N_Ae/3600\times22.4\times10^{-3}=2390 \text{ Ah Nm}^{-3} \quad (2)$$

The H_2 yield rate (R) was calculated from Eq. 3 .

$$R=j/Q \text{ Nm}^3\text{h}^{-1}\text{ m}^{-2} \quad (3)$$

1.7. Techno-economic analysis (TEA)

Our techno-economic analysis (TEA) model follows a general framework established in prior research. We evaluated the costs for producing 20 tonnes per day over a 30-year operational plant lifetime. To estimate the operational voltage for a potential industrial electrolyzer, we utilized an experimentally derived membrane electrode assembly (MEA) cell voltage of V_{cell} and a total current density of I A/cm², as determined from our stability experiments.

Cathode reaction: $4H_2O + 4e^- \rightarrow 4OH^- + 2H_2$

Anode reaction: $4OH^- \rightarrow O_2 + 4e^- + 2H_2O$

Overall reaction: $2H_2O \rightarrow O_2 + 2H_2$

Therefore, producing 1 mole of H_2 requires 0.5 mole of H_2O.

1.7.1 Electricity:

The production rate of hydrogen in moles per second is:

$$H_{2Production}\left(\frac{mol}{s}\right) = \frac{H_2\ Prodcution}{M_{H_2}\frac{g}{mol}} = \frac{20\times\frac{10^6}{g}}{\frac{2g}{mol}\times\frac{86400s}{day}} = 115.75\frac{mol}{s}$$

Considering the loss of electrons due to FE below 100%, we find the current needed to produce hydrogen at the target production rate:

$$I_{Total}(A) = \frac{H_{2Production}(\frac{mol}{s}) \times n \times F}{98\%} = \frac{115.75\frac{mol}{s} \times 2 \times 96485\frac{sA}{mol}}{98\%} =$$

We multiply the experimentally derived MEA cell voltage V_{cell} and energy efficiency of 72.45% by the current to calculate the power consumption.

$$\text{Power (kW)} = I_{Total}(A) \times \frac{V_{cell}}{1000 \times 72.45\%} kW = 56627.36\ kW$$

To determine the energy consumption for producing 20 tonnes of hydrogen, we multiply the power requirement by 24 hours. We assume the energy efficiency is 72.45%. The resulting energy consumption is then multiplied by the electricity rate (0.012 $/kWh) to calculate the cost per tonne of hydrogen produced.

$$Cost_{electricity}\left(\frac{\$}{tonne\ H_2}\right) = \frac{Power \times 24h \times price_{electricity}}{H_{2production}} = \frac{22{,}792{,}513.72\ A \times 1.8 \times 2}{1000 \times 20 \times 72.45\% t}$$

$$= 815.43\frac{\$}{tonne\ H_2}$$

1.7.2 Electrolyzer Capital Cost:

Multiplying by the unit price of the electrolyzer (450 $/kW) and scaling by the current density, we obtain the total cost of the electrolyzer, according to the reference electrolyzer cost of 450 $/kW, and current density of 400 mA cm^{-2}.

$$Cost_{Total\ Electrolyzer}(\$) = Power\ Consumed\ (kW) \times Cost_{Electrolyzer}(\$) \times \frac{base\ cu}{input\ curre}$$

$$= 56627.36\ kW \times 450\frac{\$}{kW} \times \frac{400}{500} = 20385849.6\$$$

This method of converting long-term investments into daily costs is applied to all capital expenses, using a capital recovery factor (CRF) calculated based on a discount rate of 7% and a material lifespan of 20 years.

$$CRF_{electrolyzer} = \frac{i(1+i)^{lifetime}}{(1+i)^{lifetime}-1} = \frac{0.07(1.07)^{20}}{(1.07)^{20}-1} = 0.094393$$

Next, the total capital cost of the electrolyzer is multiplied by the CRF, then divided by the number of operational days and the daily hydrogen output. In all calculations, it is assumed that the plant operates at a capacity factor of 0.9.

$$Cost_{electrolyzer}\frac{\$}{tonne\ H_2}$$
$$= \frac{CRF_{electrolyzer} \times Cost_{Total\ electrolyzer}(\$)(\frac{mA}{cm^2})}{Capacity\ factor \times 365(\frac{day}{year}) \times production(\frac{tonne\ H_2}{day})}$$
$$= \frac{0.094393 \times 20385849.6}{0.9 \times 365(\frac{day}{year}) \times 20(\frac{tonne\ H_2}{day})} = 292.889\frac{\$}{tonne\ H_2}$$

1.7.3 Catalyst and Membrane Costs:

For the catalyst and membrane costs, we assume they account for 5% of the total electrolyzer cost. The cost per tonne of hydrogen is calculated based on a catalyst and membrane lifetime of 5 years:

$$CRF_{C\&M} = \frac{i(1+i)^5}{(1+i)^5-1} = 0.24389$$

$$Cost_{C\&M}\frac{\$}{tonne\ H_2}$$
$$= \frac{CRF_{C\&M} \times Cost_{Total\ Electrolyzer}(\$) \times 5\%}{Capacity\ factor \times 365\frac{days}{year} \times production(\frac{tonne\ H_2}{day})} = \frac{0}{0.}$$
$$= 37.83\frac{\$}{tonne\ H_2}$$

1.7.4 Input water:

The required amount of water was calculated using the same method. Now, multiplying this by the cost of treated seawater (10 $/tonne) and dividing by the daily hydrogen production gives us the final cost of the input water as follows:

$$H_2O_{required}\frac{tonne\ H_2O}{day}$$

$$= product\ output\left(\frac{tonne\ product}{day}\right) \times \frac{M_{H_20}}{M_{H_2}} \times molar\ ratio\left(\frac{H_20}{product}\right)$$

$$= 20\left(\frac{tonne\ product}{day}\right) \times \frac{18}{2} \times \frac{1}{1}\left(\frac{H_20}{product}\right)\frac{tonne\ H_2O}{day}$$

$$= 180\frac{tonne\ H_2O}{day}$$

$$Cost_{treated\ seawater}(\frac{\$}{tonne\ H_2})$$

$$= 10\frac{\$}{tonne\ H_2} \times 180\frac{tonne\ H_2O}{day} \times \frac{1}{20\ tonne\frac{H_2}{day}} = \frac{90\$}{tonne\ H_2}$$

1.7.5 Electrolyte cost:

Our electrolyte consists of 1.0 M KOH seawater. By applying a fixed volume ratio of 100 L of electrolyte per square meter of electrolyzer, we can calculate the total volume of electrolyte required for the system.

$$Volume_{electrolyte}(L)$$

$$= Surface\ area_{electrolyzer}(m^2) \times \frac{L}{m^2} = \frac{Total\ curren}{Current\ density\frac{A}{cm^2}} \times$$

$$\times 100\frac{L}{m^2} = \frac{Total\ current\left(\frac{A}{s}\right)}{I\frac{A}{cm^2} \times \left(\frac{100\ cm}{1\ m}\right)^2} \times 100\frac{L}{m^2} = 455850.28L$$

$$Mass_{KOH}(g)$$

$$= molarity_{KOH}\left(\frac{mol}{L}\right) \times Volume_{electrolyte}(L) \times molecular\ wei$$

$$= 1\frac{mol}{L} \times 455850.28L \times 56.11\frac{g}{mol} = 25577759.2108g$$

$$Cost_{electrolyte}(\$) = Mass_{KOH}(tonne) \times price_{KOH}\left(\frac{\$}{tonne}\right) + Volume_{water}(L) \times p$$

$$\left(\frac{\$}{tonne}\right)$$

$$= 25.57 onne \times 790\frac{\$}{tonne} + 455850.28L \times \frac{1 \quad tonne}{1000 \quad L} \times 5\frac{}{to}$$

$$= 22479.55\$$$

To determine the cost per tonne of hydrogen, we calculate a new CRF of 1.07, assuming an electrolyte lifetime of one year. This allows us to estimate the electrolyte costs per tonne of hydrogen produced.

$$Cost_{electrolyte}\frac{\$}{tonne\ H_2} = \frac{CRF_{electrolyzer} \times Cost_{electrolyte}(\$)}{Capacity\ factor \times 365\frac{days}{year} \times production(\frac{tonne\ H_2}{day})} =$$

$$\frac{1.07 \times 22479.55\$}{0.9 \times 365\frac{days}{year} \times 20(\frac{tonne\ H_2}{day})} = 3.66\frac{\$}{tonne\ H_2}$$

1.7.6 Balance of Plant and Installation:

All capital costs are adjusted to estimate the price of peripheral equipment surrounding the electrolyzer and separation units. We assume a balance of plants (BOP) at 50% and apply a Lang factor of 1. To calculate the total capital costs, we sum the expenses for the electrolyzer, membrane and catalyst, as well as the cathode separation equipment.

$$Cost_{Total\ capital}\left(\frac{\$}{tonne\ H_2}\right) = Electrolyzer\ cost\ +\ Catalyst\ cost = 292.889 + 37.83\frac{\$}{tonne\ H_2}$$

$$= 330.719\frac{\$}{tonne\ H_2}$$

$$Cost_{Installation}\left(\frac{\$}{tonne\ H_2}\right) = Lang\ Factor \times Cost_{Total\ capital} = 330.719\frac{\$}{tonne\ H_2}$$

$$BOP\left(\frac{\$}{tonne\ H_2}\right) = BOP\ Factor \times Cost_{Total\ capital} = 165.35\frac{\$}{tonne\ H_2}$$

1.7.7 Other operating costs:

To account for the additional operating expenses related to running the factory (including labor and maintenance), we have included an extra charge equal to 10% of the electricity cost:

$$Cost_{other\ operation}\left(\frac{\$}{tonne\ H_2}\right)$$
$$= Cost_{electricity}\left(\frac{\$}{tonne\ H_2}\right) \times 0.1 = 815.43 \times 0.1\frac{\$}{tonne\ H_2}$$
$$= 81.54\frac{\$}{tonne\ H_2}$$

1.7.8 Total cost for one tonne of hydrogen:

By adding up all the aforementioned costs, we can determine the total cost of producing one tonne of hydrogen using an electrolyzer.

$$Cost_{H_2}$$
$$= Cost_{electricity} + Cost_{electrolyzer} + Cost_{catalyst+membrane} + C$$
$$+ Cost_{electrolyte} + BOP + Cost_{operation} + Cost_{installation}$$
$$= 815.43 + 292.889 + 37.83 + 90 + 3.66 + 165.35 + 81.54$$
$$+ 330.719\frac{\$}{tonne\ H_2} = 1817.42\frac{\$}{tonne\ H_2}$$

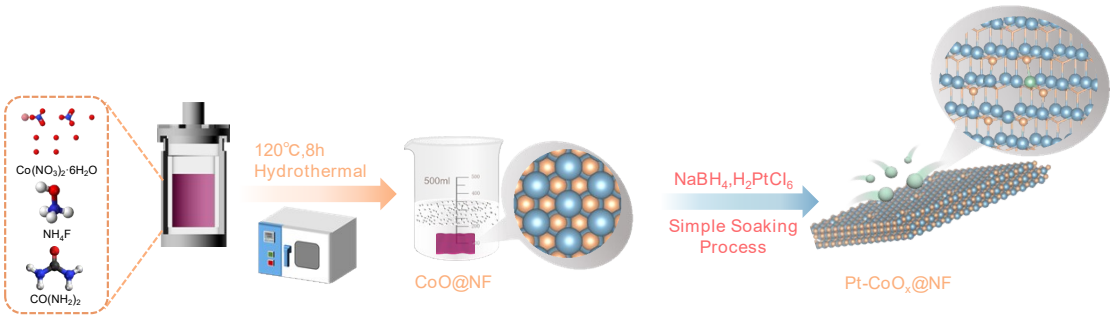

Figure S1. Schematic diagram of Pt-CoO_x synthesis.

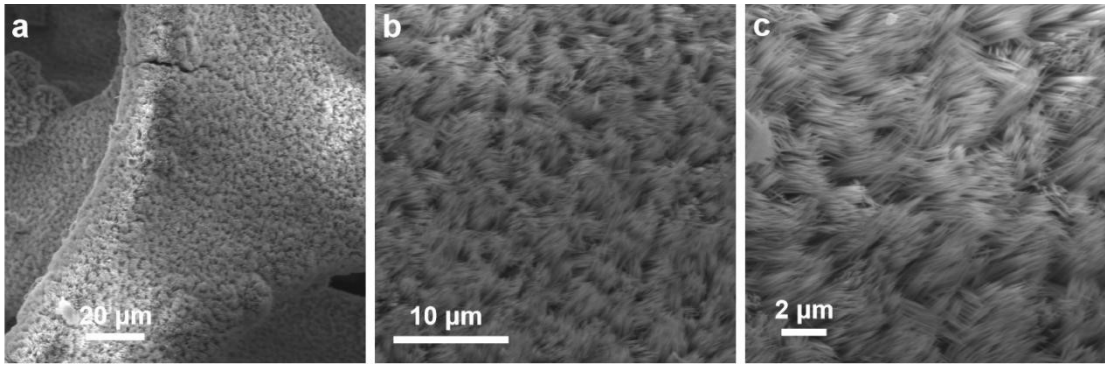

Figure S2. (a-c) SEM images of CoO.

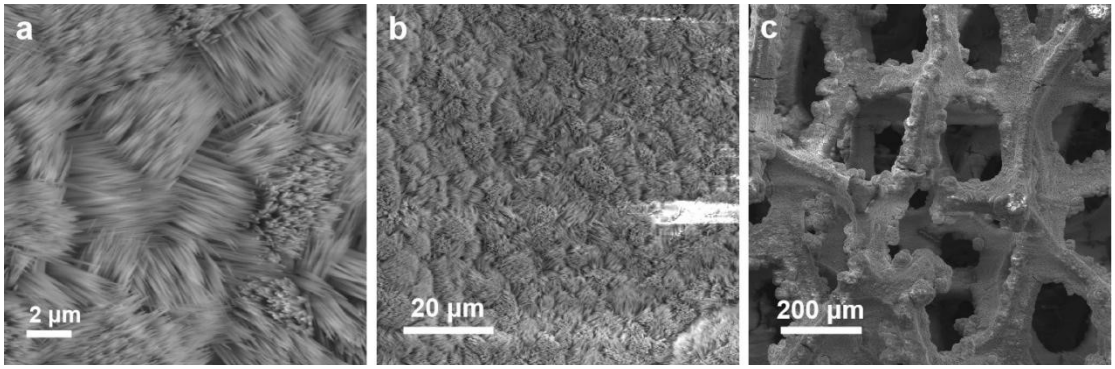

Figure S3. (a-c) SEM images of Pt-CoO_x.

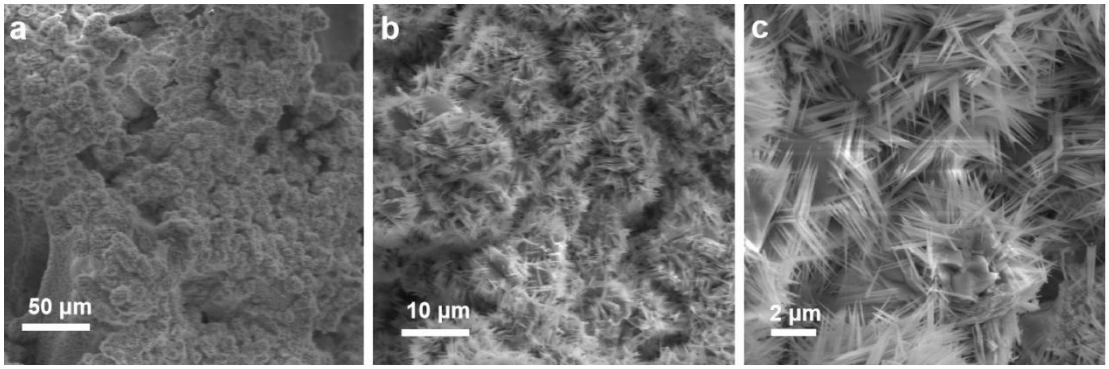

Figure S4. (a-c) SEM images of Pt-CoO.

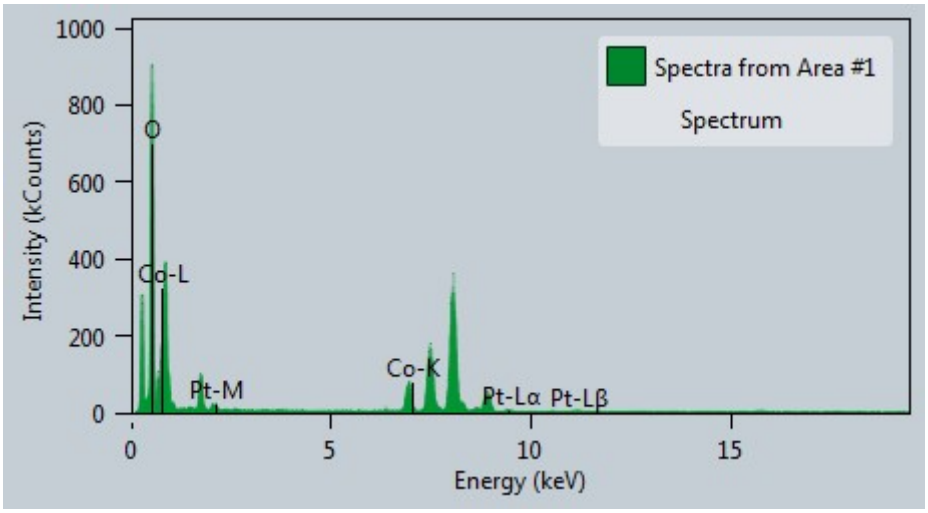

Figure S5. The EDS spectrum of Pt-CoO_x.

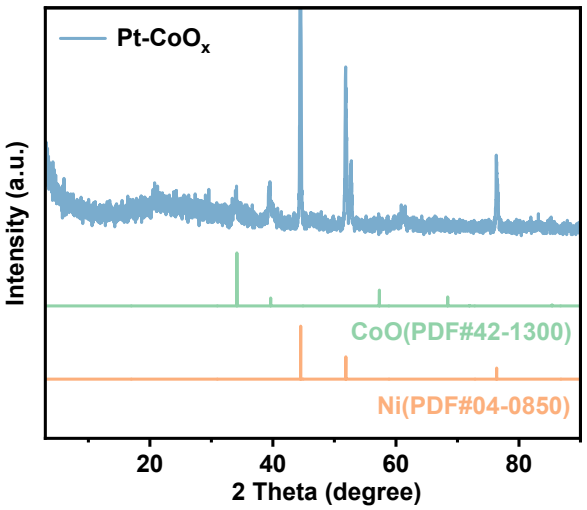

Figure S6. XRD pattern of Pt-CoO_x.

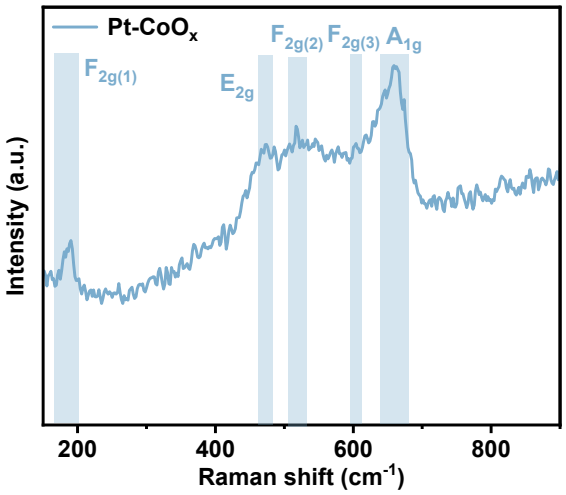

Figure S7. Raman spectra of Pt-CoO_x.

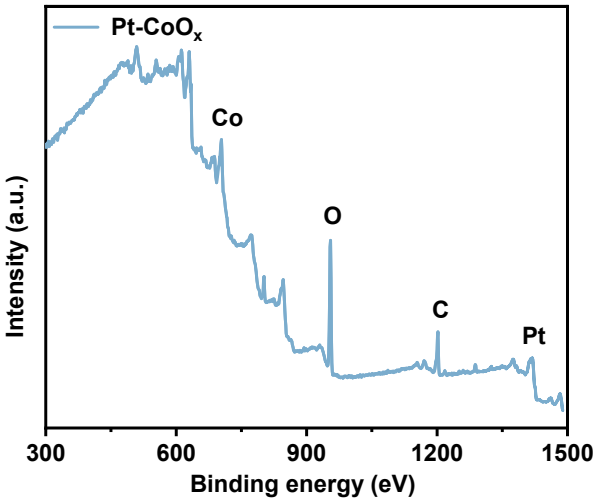

Figure S8. XPS survey spectra of Pt-CoO_x.

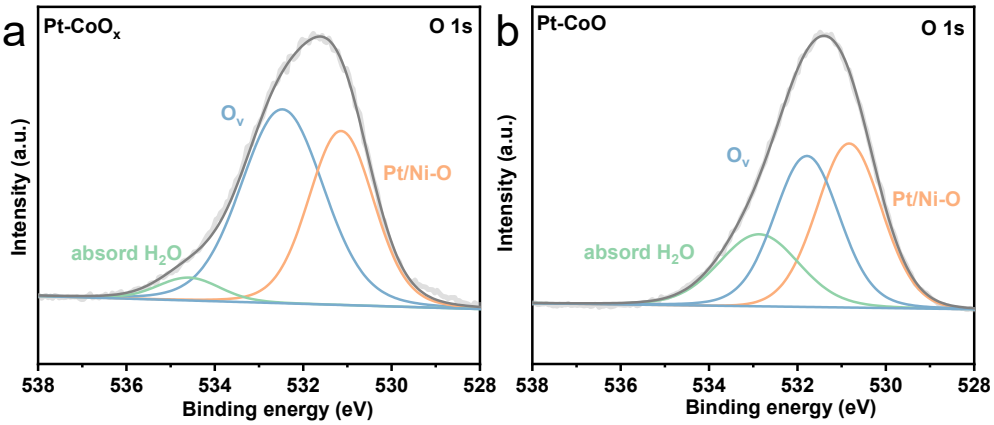

Figure S9. O 1s XPS spectra of (a) Pt-CoO_x and (b) Pt-CoO.

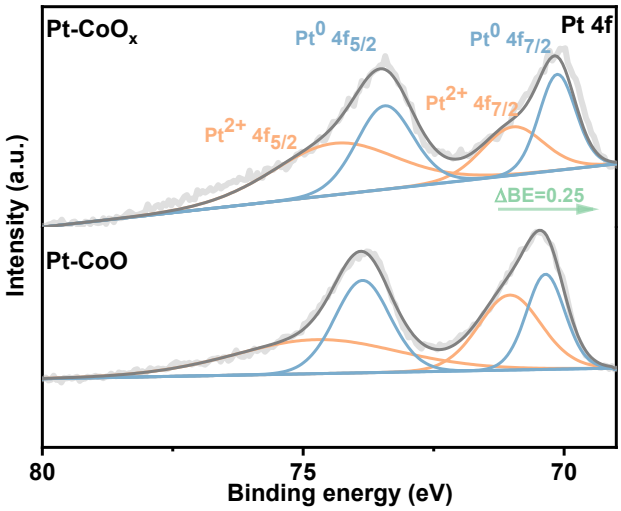

Figure S10. Pt 4f XPS spectra of Pt-CoO_x and Pt-CoO.

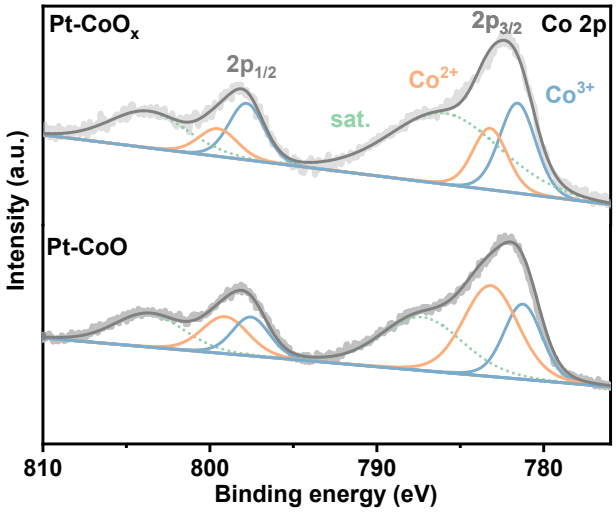

Figure S11. Co 2p XPS spectra of Pt-CoO_x and Pt-CoO.

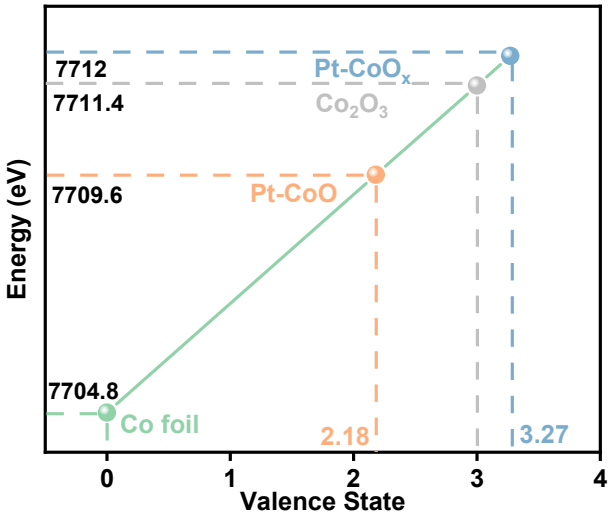

Figure S12. XANES valence state fitting line graph.

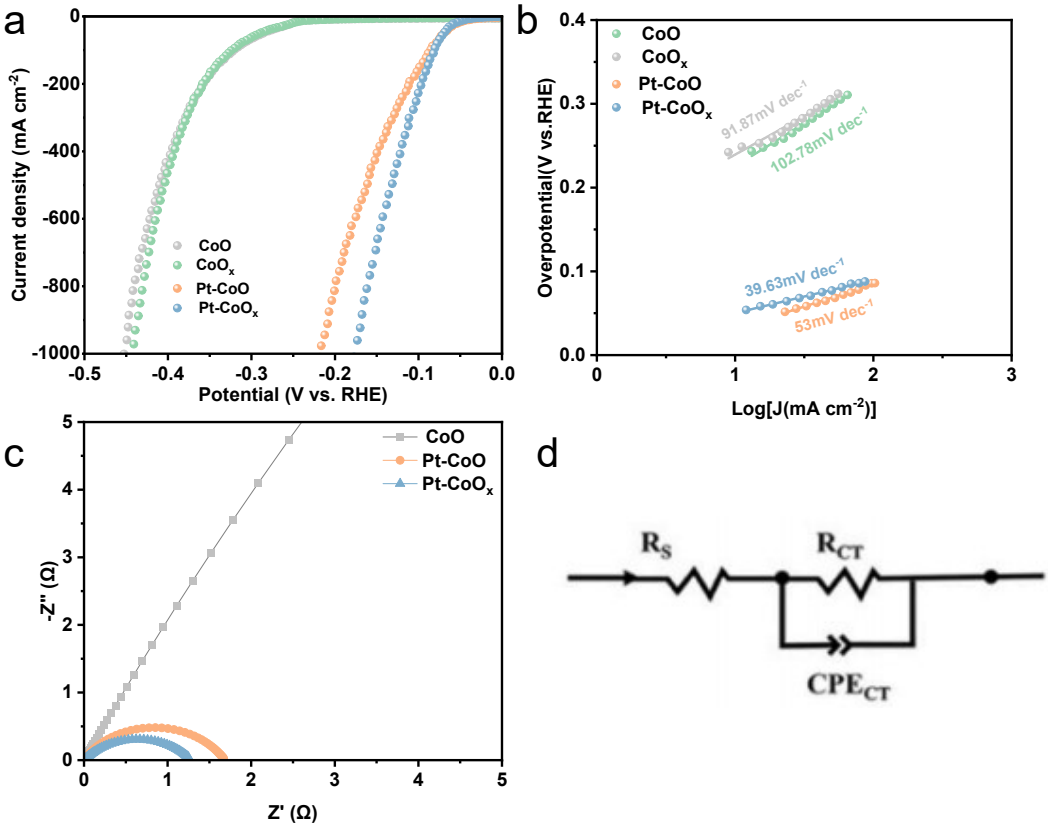

Figure S13. (a) LSV curves, (b) Tafel slope plots, (c) EIS and (d) the equivalent circuit model used in the fitting of the impedance data in 1.0 M KOH.

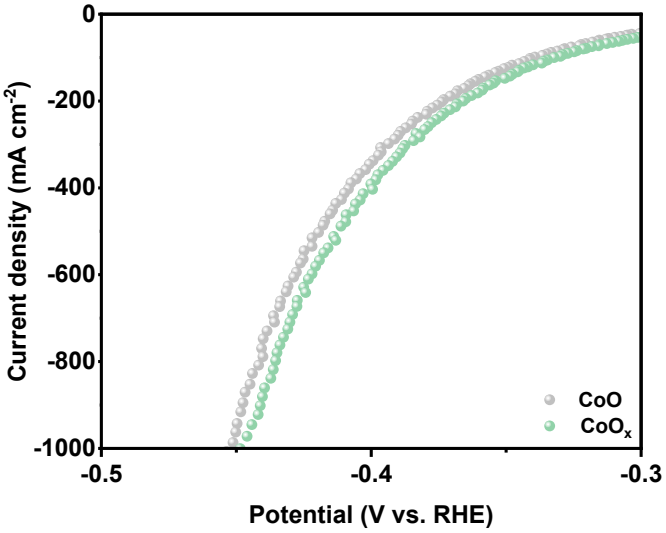

Figure S14. LSV curves in 1.0 M KOH + seawater electrolyte.

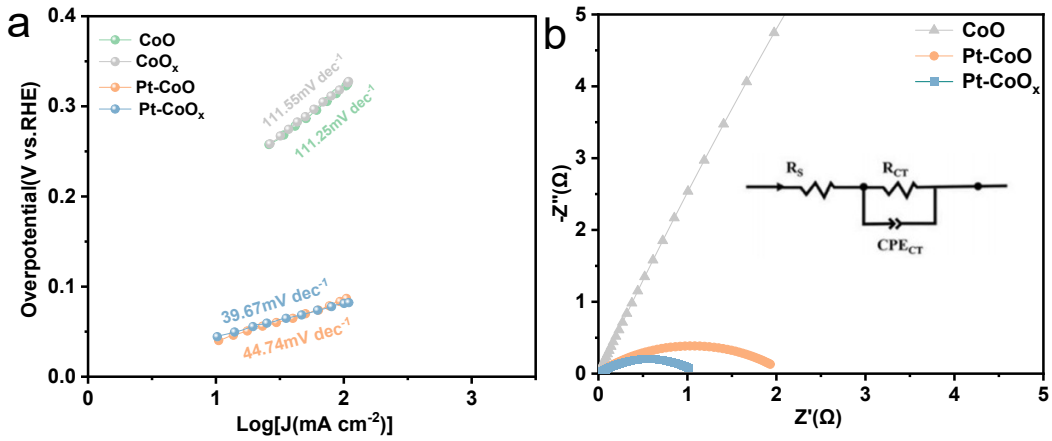

Figure S15. (a) The Tafel slope plots and (b) EIS in 1.0 M KOH + seawater electrolyte.

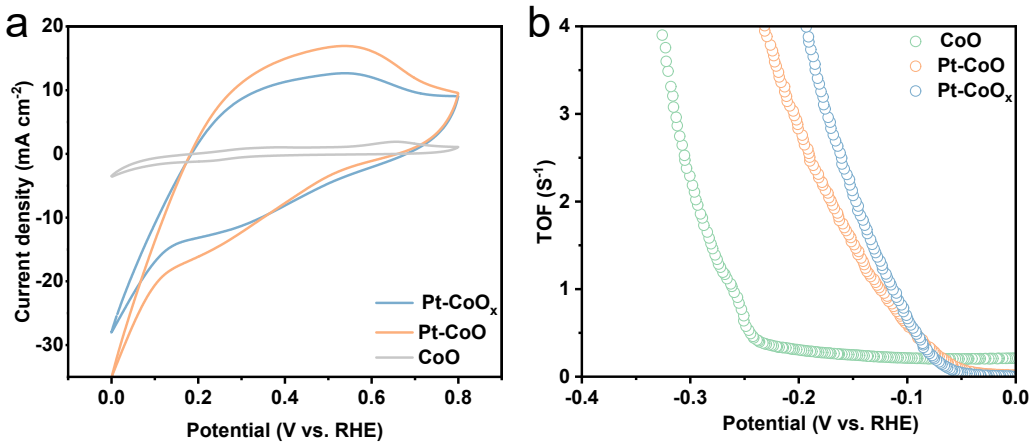

Figure S16. (a) The CV of ECSA and (b) TOF curves in PB electrolyte.

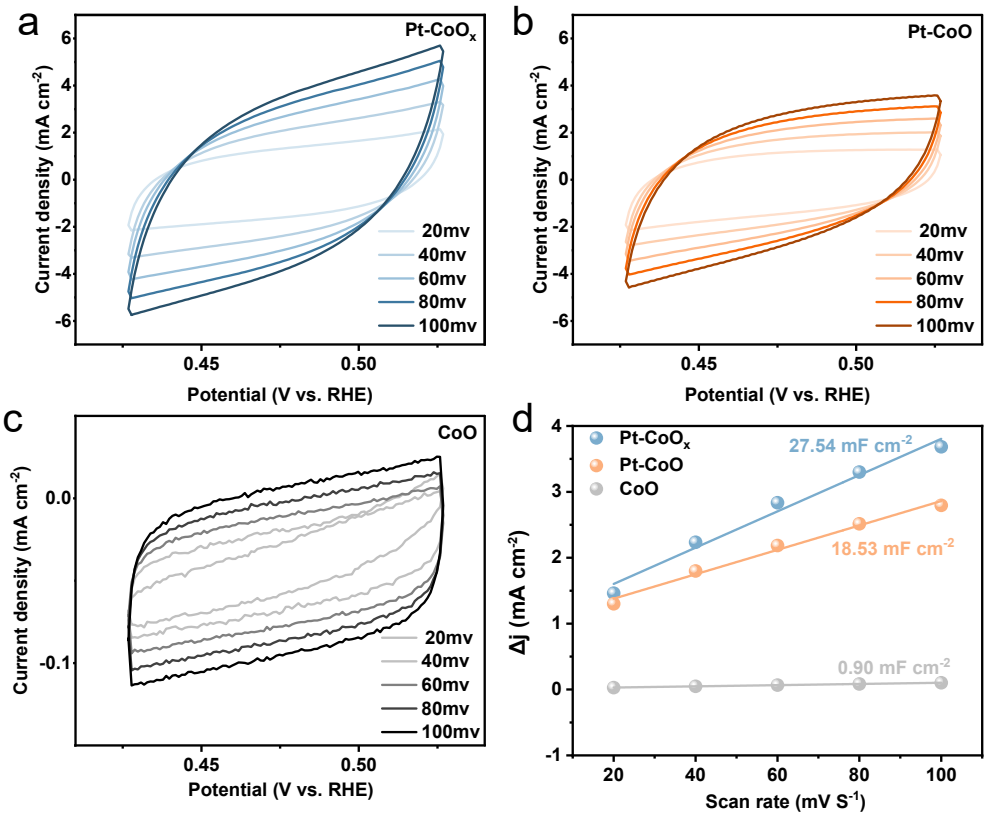

Figure S17. (a) CV curves of Pt-CoO_x catalyst for ECSA, (b) CV curves of Pt-CoO catalyst for ECSA and (c) CV curves of CoO catalyst for ECSA in 1.0 M KOH + seawater. (d) The C_{dl} values in 1.0 M KOH + seawater electrolyte.

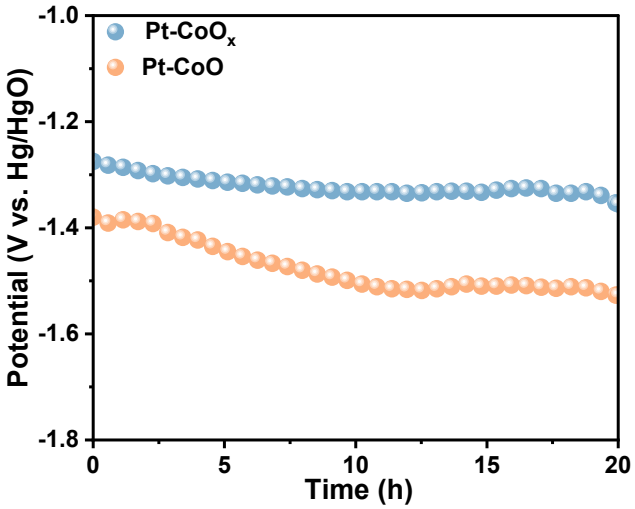

Figure S18. U-t curves for HER in 1.0 M KOH + seawater electrolyte.

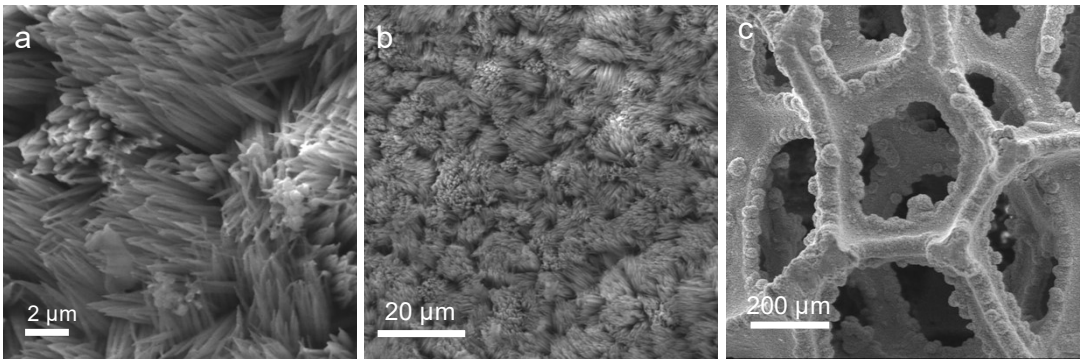

Fig. S19. (a-c) SEM images of Pt-CoO_x after 20 hours stability tests.

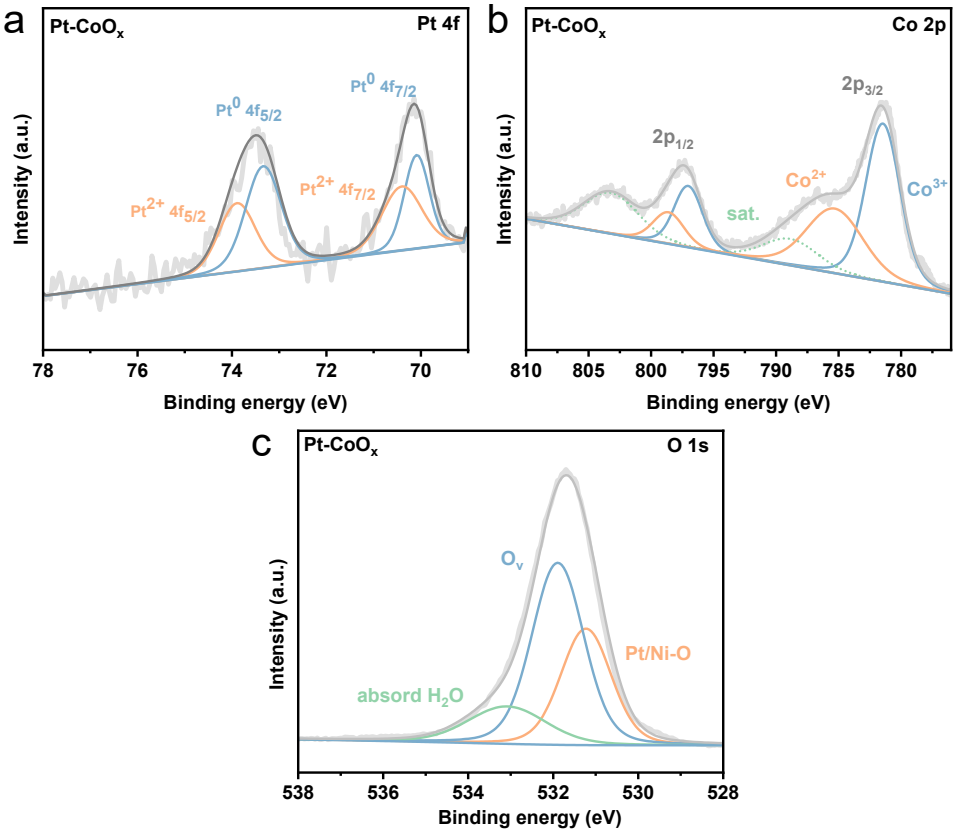

Fig. S20. XPS spectra of Pt-CoO_x (a) Pt 4f (b) Co 2p (c) O 1s after 20 hours stability tests.

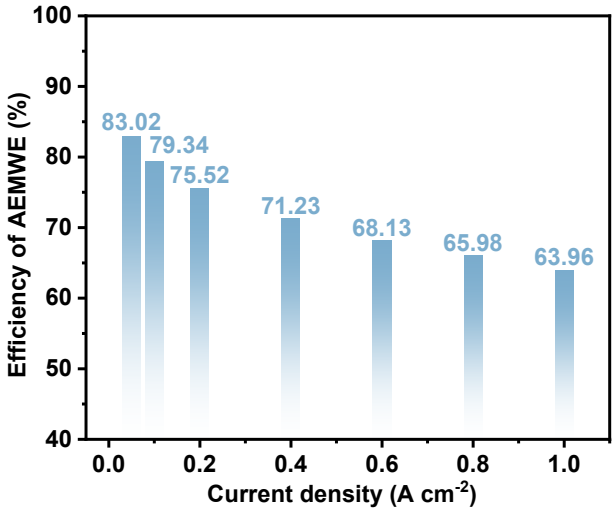

Figure S21. Efficiency of AEMWE at various current densities.

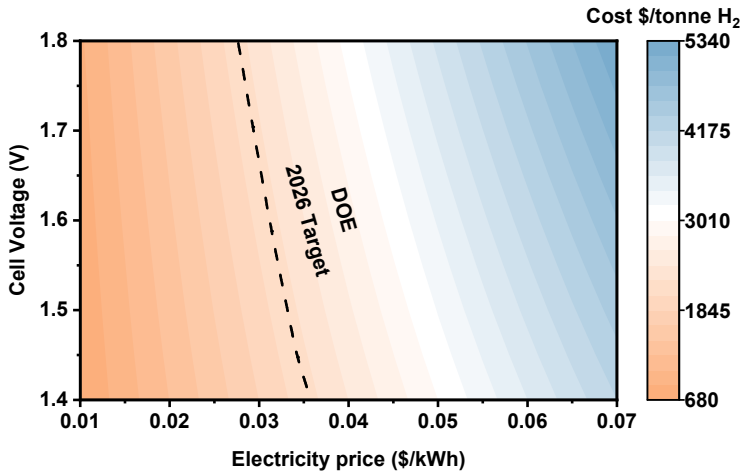

Figure S22. Effect of cell voltage and electricity price fluctuations on hydrogen production cost.

Note 1: The electricity cost was estimated from the total energy required to produce 20 tons of hydrogen, assuming an energy efficiency of 72.45% and an electricity price of 0.012 USD kWh^{-1}. The capital cost of the electrolyzer was set at 450 USD kW^{-1}, operated at 400 mA cm^{-2} with a 7% discount rate and a 20 year service life. This value was then converted into the hydrogen production cost per ton using the capital recovery factor (CRF). Catalysts and membranes account for approximately 5% of the electrolyzer cost and are assumed to have a lifetime of five years. The costs of water and electrolyte were calculated based on their consumption, with seawater treatment estimated at 10 USD per ton. In addition, the BOP system cost was estimated as 50% of the electrolyzer cost, and the total capital investment was adjusted using the Lang factor. Routine operating expenses were taken as 10% of the electricity cost.[3]

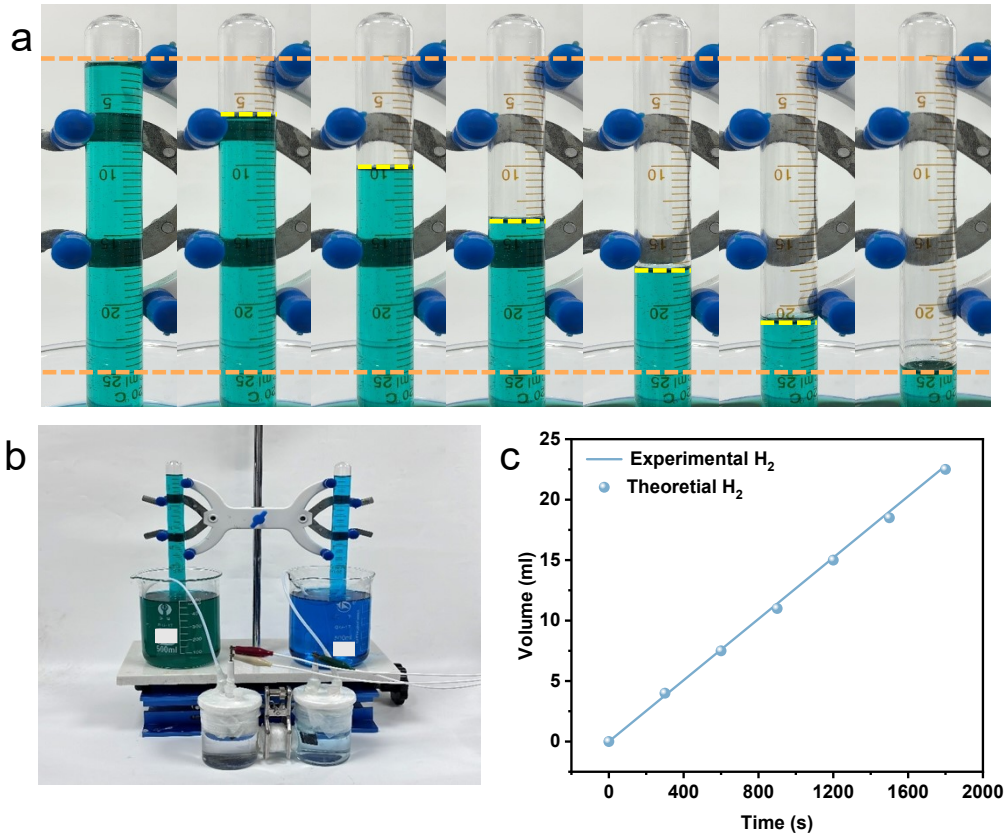

Figure S23. (a) The corresponding photographs of the gas of H_2 varying with time in alkaline seawater. (b) The gas collection device of alkaline seawater splitting. (c) Faradaic efficiency of Pt-CoO_x at 100 mA cm^{-2}.

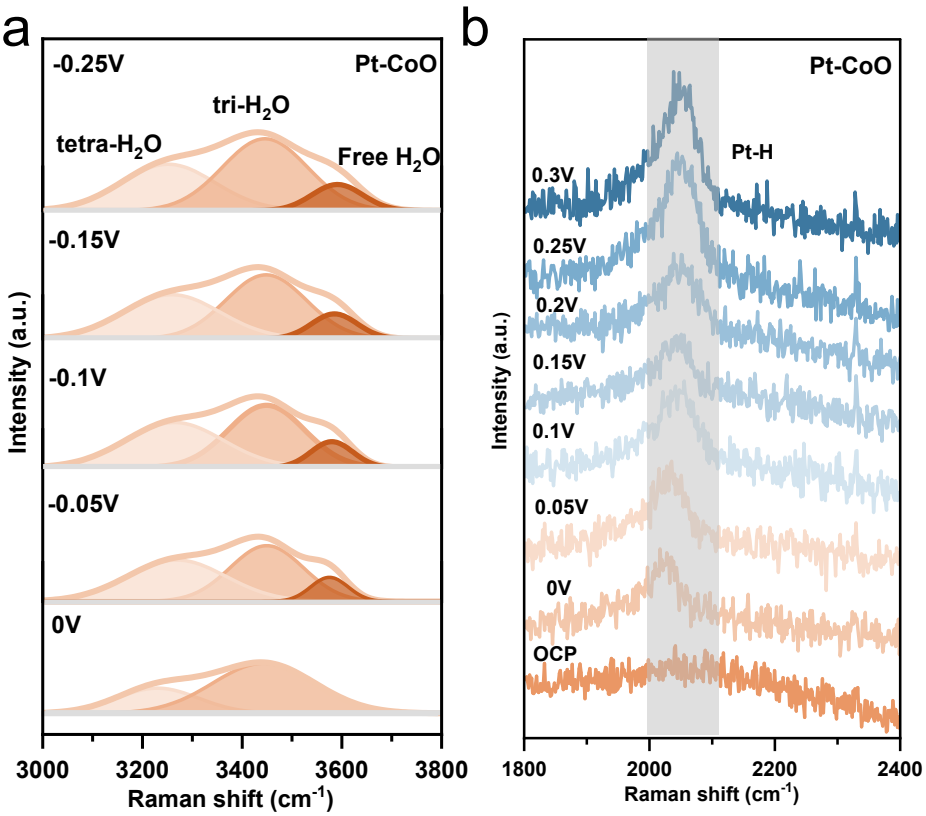

Figure S24. (a) Raman spectrum of the Pt-CoO catalyst showing the water-related peak. (b) In situ Raman spectra of Pt-CoO catalyst.

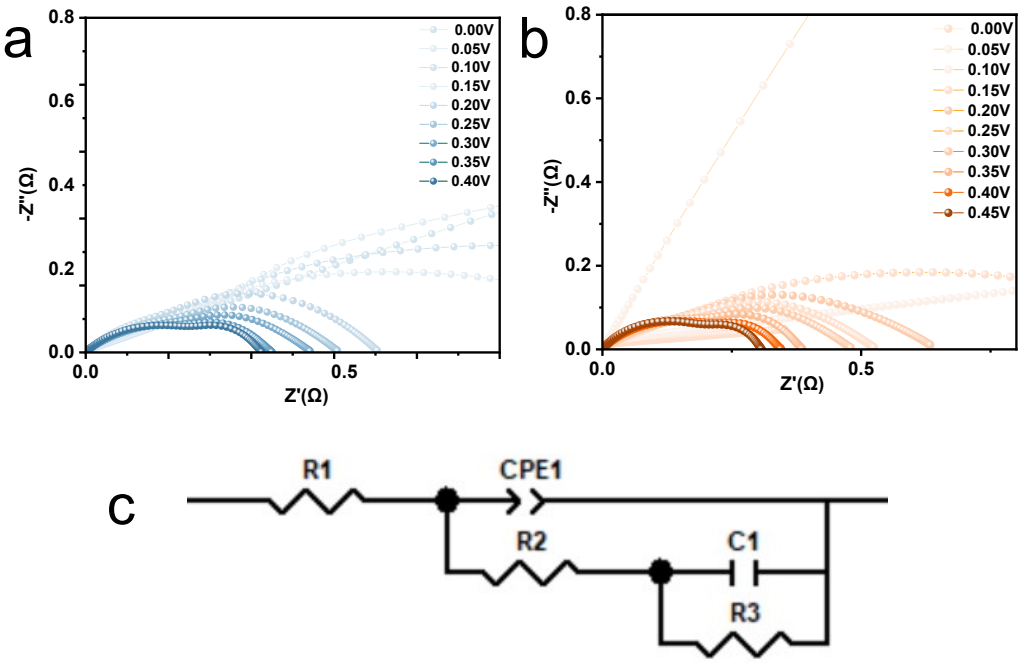

Figure S25. Nyquist plots for (a) Pt-CoO_x and (b) Pt-CoO at different applied potentials for HER. (c) The equivalent circuit model used in the fitting of the impedance data.

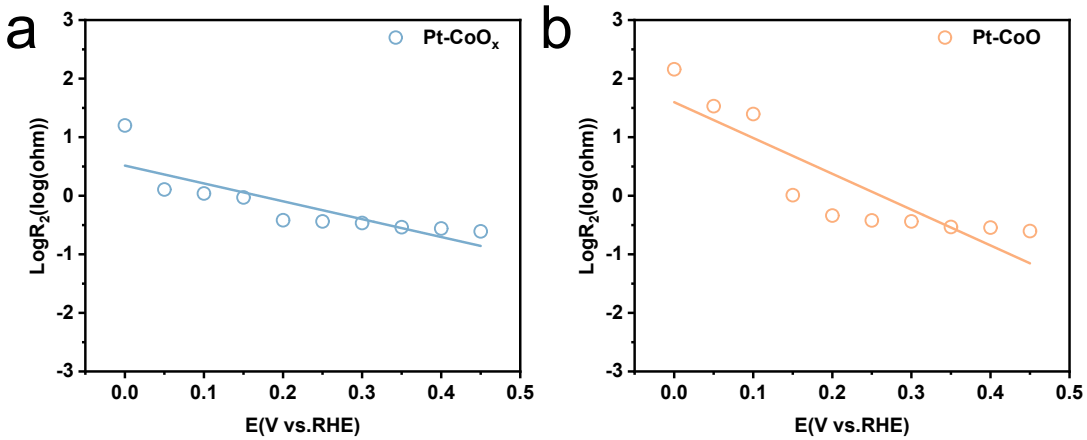

Figure S26. EIS-derived Tafel plots for (a) Pt-CoO_x and (b) Pt-CoO catalyst.

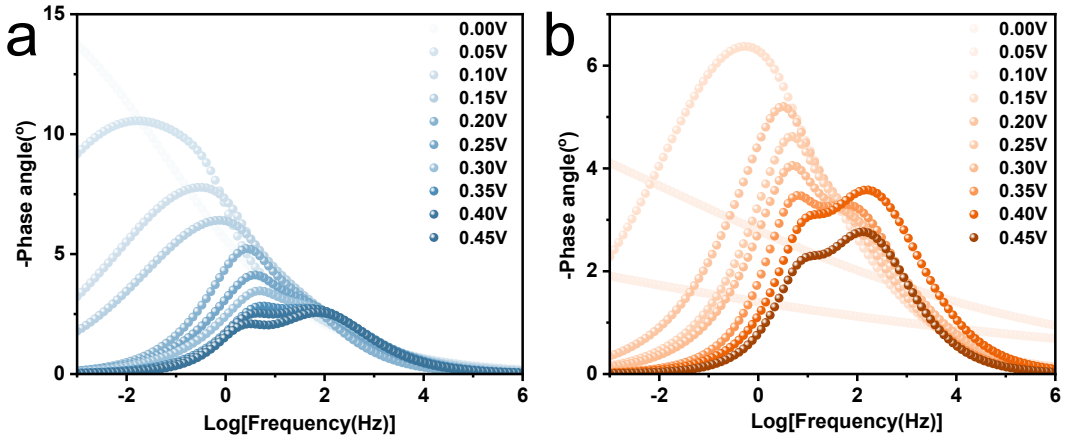

Figure S27. Bode-phase plots of (a) Pt-CoO_x and (b) Pt-CoO under different operated potentials (vs RHE).

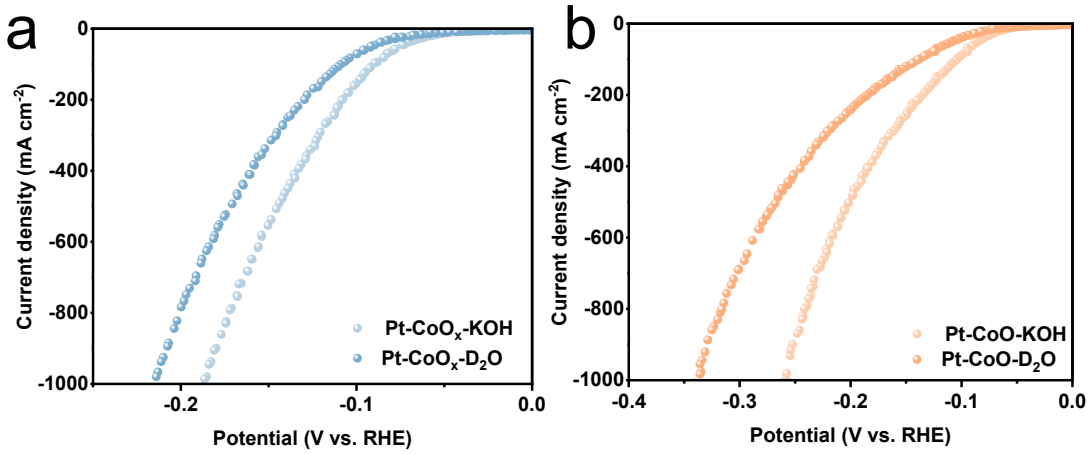

Figure S28. HER polarization curves of (a) Pt-CoO_x and (b) Pt-CoO in alkaline ultrahigh-purity H_2O and D_2O.

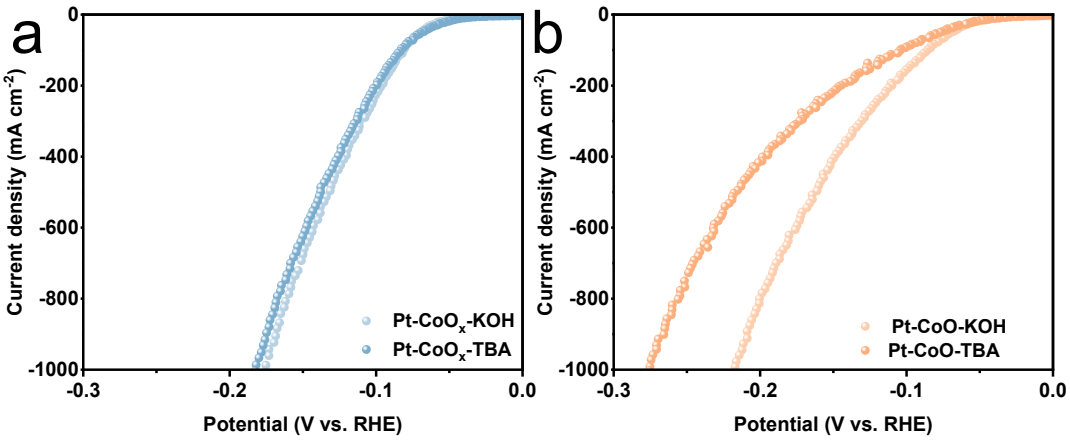

Figure S29. Different LSV curves of (a) Pt-CoO_x and (b) Pt-CoO with or without 1.0 M TBA.

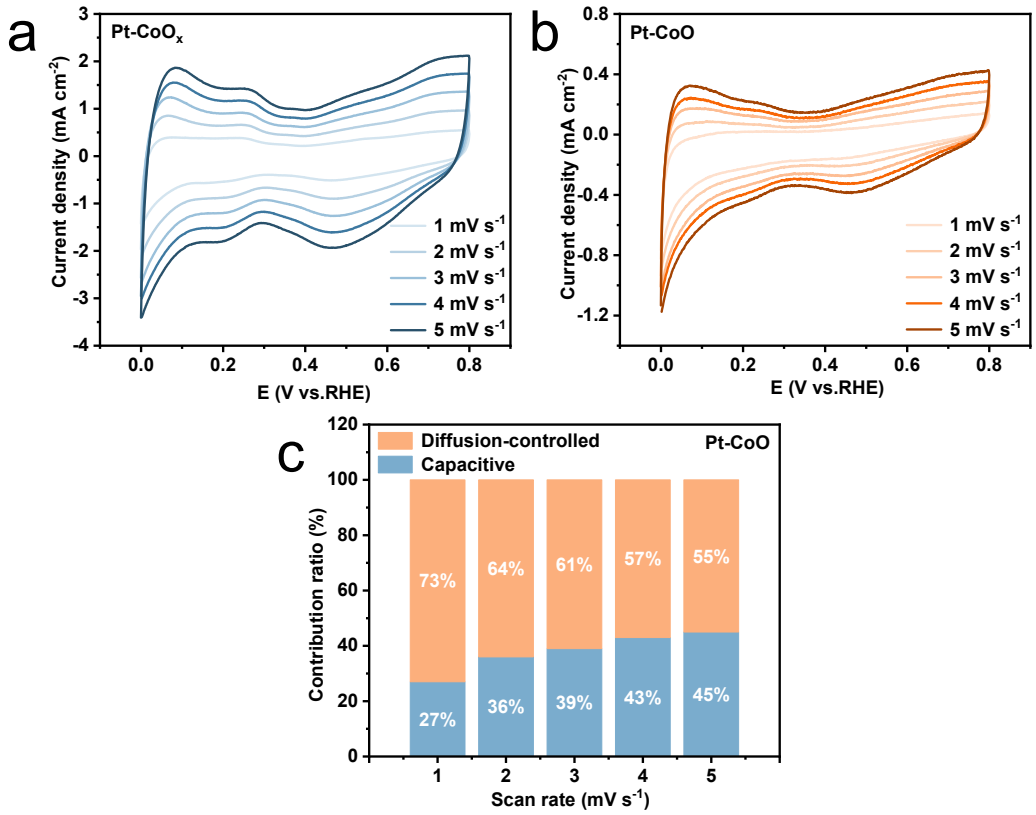

Figure S30. CV curve of (a) Pt-CoO$_x$ and (b) Pt-CoO in 1.0 M KOH + seawater electrolyte. (c) Pt-CoO contribution rate of pseudocapacitance derived from the CV curve calculation.

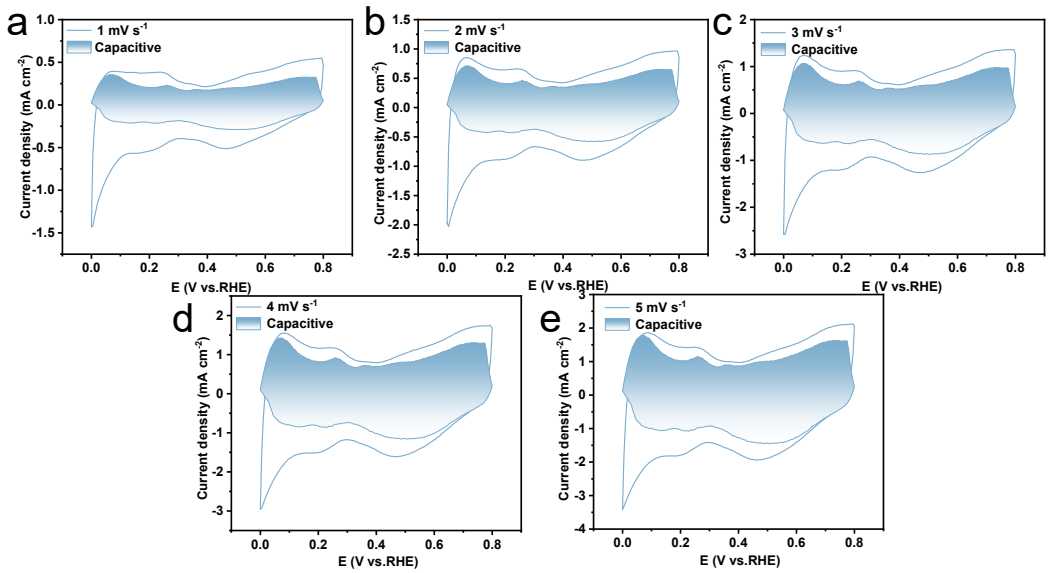

Figure S31. (a-e) Graph of contribution rate of pseudocapacitance of Pt-CoO_x at different scanning rates.

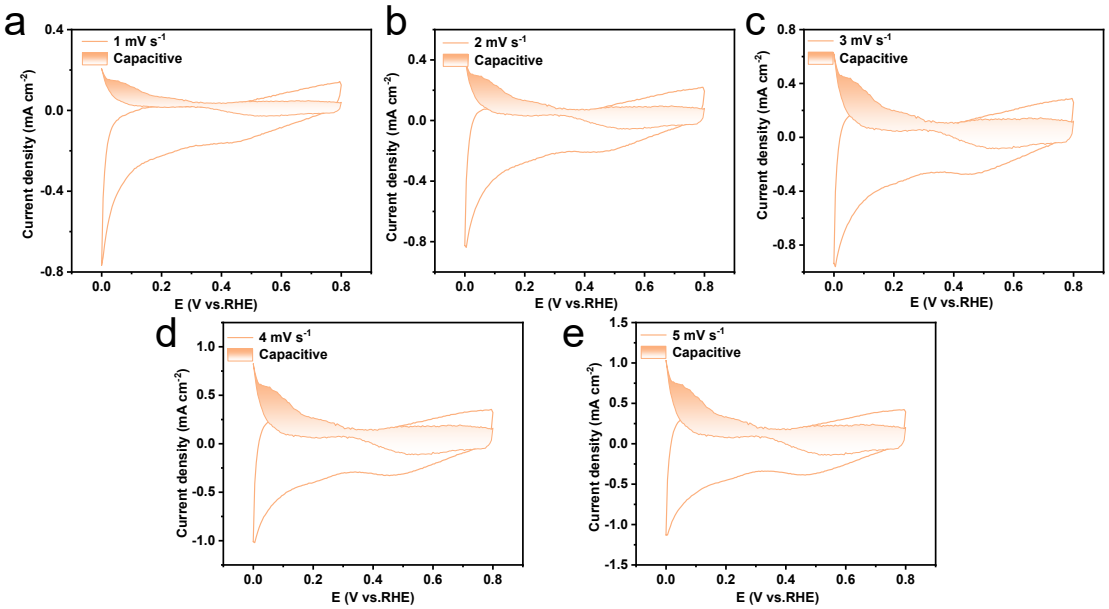

Figure S32. (a-e) Graph of contribution rate of pseudocapacitance of Pt-CoO at different scanning rates.

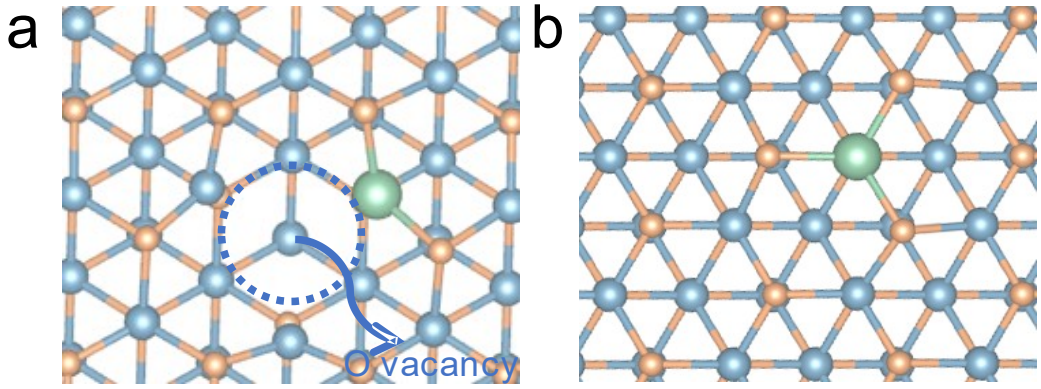

Figure S33. The perfect structure of (a) Pt-CoO_x and (b) Pt-CoO.

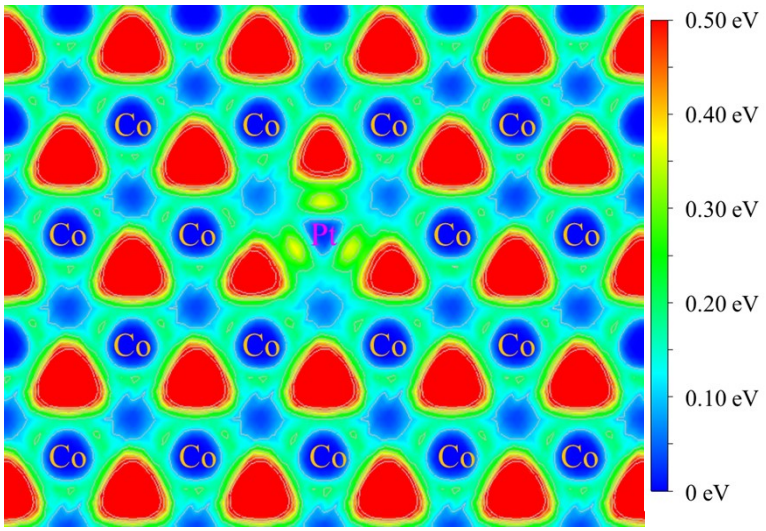

Figure S34. Electron locational function plot for Pt-CoO.

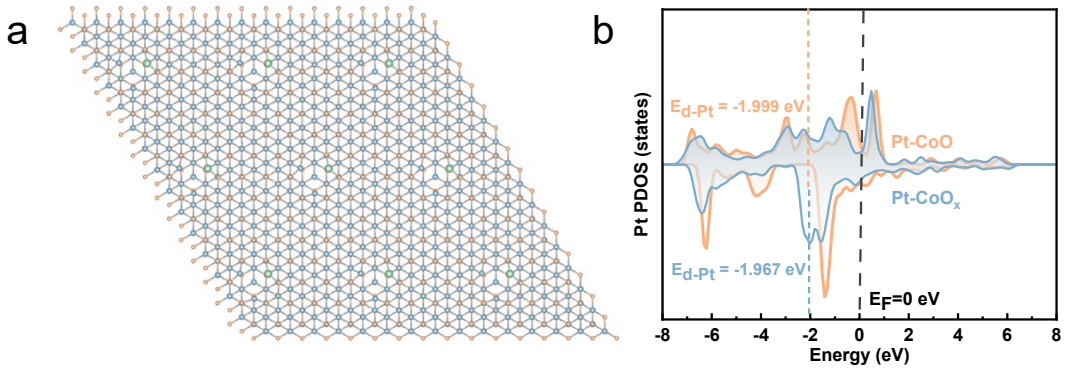

Figure S35. (a) The atomic structure model and (b) PDOS of Pt-CoO_x for HER.

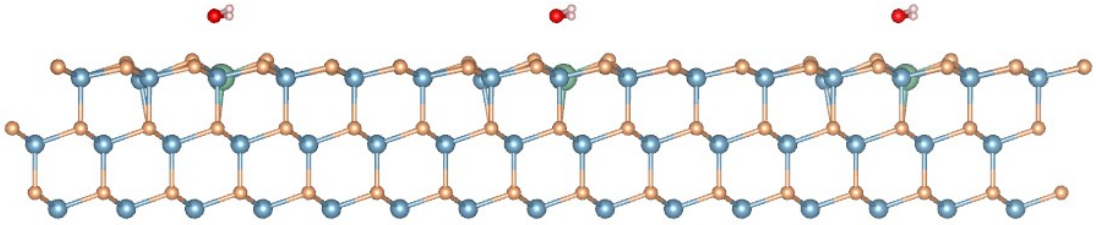

Figure S36. H_2O dissociation modeling of Pt sites on Pt-CoO_x.

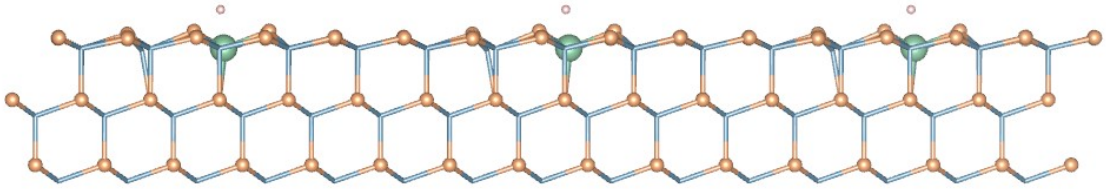

Figure S37. H adsorption modeling of Pt sites on Pt-CoO_x.

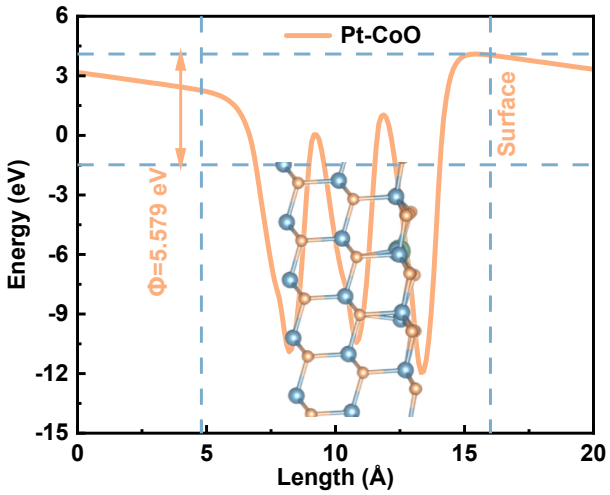

Figure S38. The computed work functions of Pt-CoO.

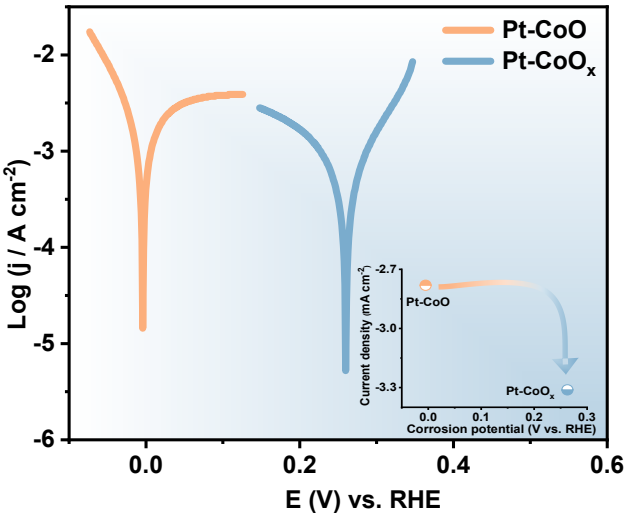

Figure S39. The corrosion polarization curve of Pt-CoO_x and Pt-CoO in 1.0 M KOH + seawater electrolyte.

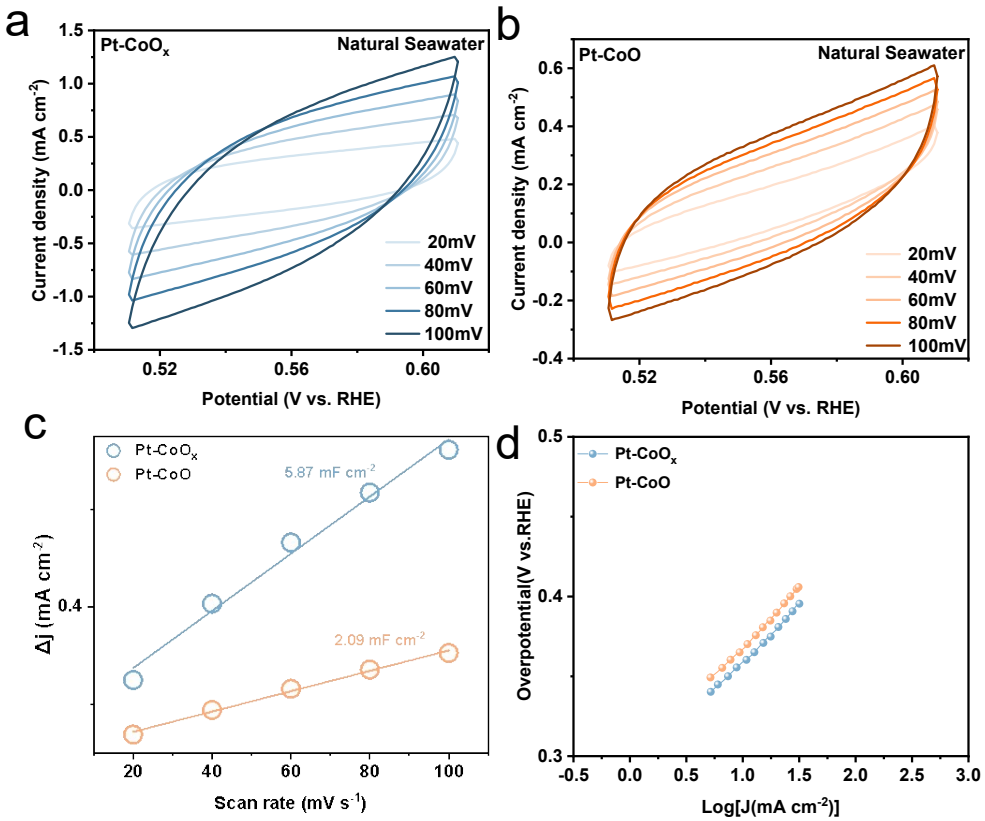

Figure S40. CV of ECSA for (a) Pt-CoO_x and (b) Pt-CoO in natural seawater. (c) The C_{dl} values of Pt-CoO_x and Pt-CoO in natural seawater. (d) The Tafel slope plots in natural seawater.

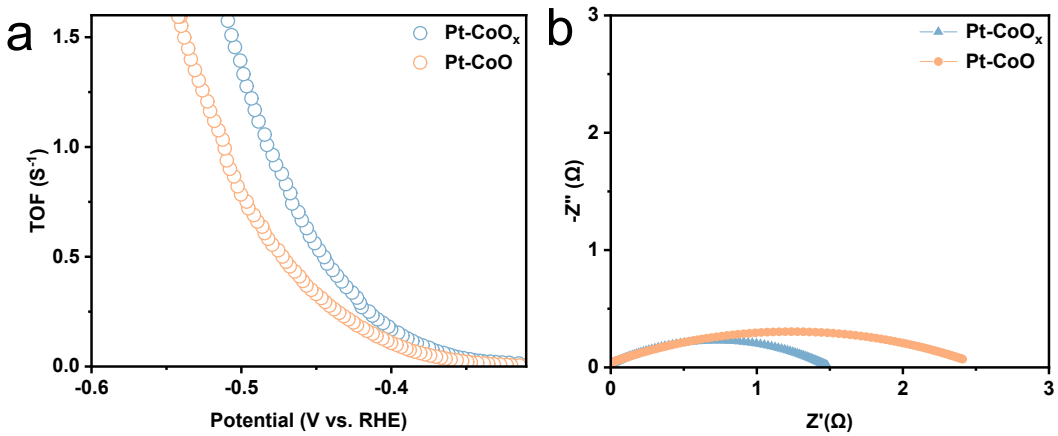

Figure S41. (a) TOF curves of Pt-CoO$_x$ and Pt-CoO. (b) EIS in natural seawater.

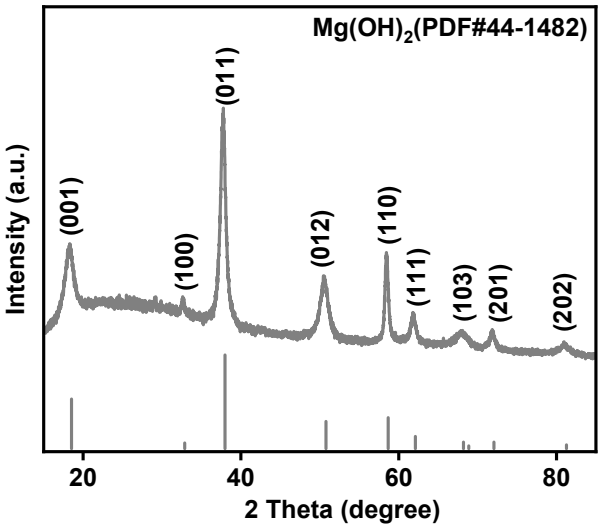

Figure S42. XRD pattern of $Mg(OH)_2$.

Table S1. Content of Pt elements of ICP in Pt-CoO_x samples.

Catalyst	Element	Mass fraction (wt%)
Pt-CoO_x	Pt	3.4439%

Table S2. Comparison with the overpotentials of recently reported HER electrocatalysts in 1.0 M KOH + seawater electrolyte.

Electrocatalyst	Electrolyte	$\eta_{100\ mA\ cm^{-2}}$ (mV)	Tafel slope(mV dec^{-1})	Ref.
Pt-CoO_x	1 M KOH+seawater	91.42	39.63	This work
Co_1/MnS_2	1 M KOH+seawater	164	45	[4]
MnCo/NiSe	1 M KOH+seawater	134.3	58.24	[5]
$(NiFeCoV)S_2$	1 M KOH+seawater	255	58.2	[6]
Cu/Co/CoO	1 M KOH+seawater	351	127.2	[7]
Co_xP_v@NC	1 M KOH+seawater	158	66.9	[8]
Ag_2Se-Ag_2S-CoCH/NF	1 M KOH+seawater	235	185.68	[9]
$NiCoHP_i$@Ni_3N/NF	1 M KOH+seawater	182	77.9	[10]
Cu_2O-CoO/CF	1 M KOH+seawater	268	83	[11]
Co-Mo-B/NF	1 M KOH+seawater	199	141	[12]
Co-P/NF	1 M KOH+seawater	213	120.2	[13]
CoP_x@FeOOH	1 M KOH+seawater	283	84.6	[14]

Table S3. Comparison with the stability of recently reported HER electrocatalysts.

Electrocatalyst	Electrolyte	[j A cm^{-2}]	Stability [h]	Ref.
S-(Ni,Fe)OOH || Pt-CoO_x	1 M KOH+seawater	-0.5	100	This work
CoFe- LDH/CoMoP/NF || CoFe-LDH/CoMoP/NF	1 M KOH+seawater	-0.1	50	[15]
Os/Ni_2P-Ni_2P_5 ‖ RuO_2	1 M KOH+seawater	-0.5	80	[16]
NiFeOOH//$(Co,Fe)PO_4$	1 M KOH+seawater	-0.1	50	[17]
	1 M KOH+seawater	-0.01		
RuO_2-NF || Act-Co-NiP_x	1 M KOH	-0.01	60	[18]
	1 M KOH+0.5 M NaCl	-0.01		
NiCoFe-Bi/NF || CO_3O_4 NS/NF	1 M KOH+seawater	-0.5	25	[19]
Co_3Mo_3N/Co_4N/Co-750 || Co_3Mo_3N/Co_4N/Co-750	1 M KOH	-0.2	100	[20]
Cu_2O-CoO/CF || Cu_2O-CoO/CF	1 M KOH	-0.1	50	[21]
Co_2P-Ni_3S_2/NF||Co_2P-Ni_3S_2/NF	1 M KOH	-0.1	24	[22]
S-$NiMoO_4$@NiFe-LDH	1 M KOH + 0.5 M NaCl,	-0.06	20	[23]
	1 M KOH+seawater	-0.06		
S-(Ni,Fe)OOH||NiCoN|NixP|NiCoN	natural seawater.	-0.01	24	[24]

Table S4. The simulated fitting results of Nyquist plots for Pt-CoO_x under different HER overpotentials.

Pt-CoO_x	R_1	CPE-1	CPE-2	R_2	C_1	R_3
0	1.111	1.672	0.2603	15.88	0.14888	4.755
0.05	1.136	1.155	0.30518	1.277	0.16182	2.944
0.10	1.168	0.81079	0.35765	1.093	0.1751	0.63612
0.15	1.187	0.68634	0.37294	0.93521	0.18174	0.30409
0.20	1.24	0.28638	0.54669	0.38173	0.21576	0.18569
0.25	1.224	0.27409	0.49858	0.3642	0.26541	0.12735
0.30	1.216	0.26178	0.47616	0.34282	0.31616	0.095891
0.35	1.221	0.17403	0.5279	0.29024	0.48873	0.071504
0.40	1.225	0.15267	0.54966	0.27582	0.73561	0.065922
0.45	1.226	0.126	0.57592	0.24626	1.118	0.060565

Table S5. The simulated fitting results of Nyquist plots for Pt-CoO under different HER overpotentials.

Pt-CoO	R_1	CPE-1	CPE-2	R_2	C_1	R_3
0	0.95345	2.82	0.062909	144.4	0.12619	6.531
0.05	1.14	0.25165	0.72046	33.83	0.15668	3.277
0.10	1.064	1.653	0.099796	24.87	0.15942	0.3437
0.15	1.096	0.79988	0.35146	1.022	0.16833	0.26201
0.20	1.108	0.37696	0.43856	0.45855	0.17422	0.19032
0.25	1.11	0.26024	0.46974	0.37914	0.17565	0.152
0.30	1.106	0.23738	0.46176	0.36506	0.23563	0.12158
0.35	1.114	0.11352	0.57248	0.29322	0.30804	0.09388
0.40	0.93887	0.082951	0.551	0.28667	0.31316	0.059772
0.45	1.268	0.063652	0.62388	0.24939	0.35553	0.058519

References

1 L. Yu, L. Wu, B. McElhenny, S. Song, D. Luo, F. Zhang, Y. Yu, S. Chen and Z. Ren, *Energy Environ. Sci.*, 2020, **13**, 3439–3446.

2 C. Feng, C. Chen, G. Xiong, D. Yang, Z. Wang, Y. Pan, Z. Fei, Y. Lu, Y. Liu, R. Zhang and X. Li, *Applied Catalysis B: Environmental*, 2023, **328**, 122528.

3 X. Yang, H. Shen, X. Xiao, Z. Li, H. Liang, S. Chen, Y. Sun, B. Jiang, G. Wen, S. Wang and L. Zhang, *Advanced Materials*, 2025, **37**, 2416658.

4 T. Sun, T. Yang, W. Zang, J. Li, X. Sheng, E. Liu, J. Li, X. Hai, H. Lin, C.-H. Chuang, C. Su, M. Fan, M. Yang, M. Lin, S. Xi, R. Zou and J. Lu, *ACS Nano*, 2025, **19**, 5447–5459.

5 R. Andaveh, A. Sabour Rouhaghdam, J. Ai, M. Maleki, K. Wang, A. Seif, G. Barati Darband and J. Li, *Applied Catalysis B: Environmental*, 2023, **325**, 122355.

6 C. Feng, M. Chen, Y. Zhou, Z. Xie, X. Li, P. Xiaokaiti, Y. Kansha, A. Abudula and G. Guan, *Journal of Colloid and Interface Science*, 2023, **645**, 724–734.

7 P. K. L. Tran, D. T. Tran, D. Malhotra, S. Prabhakaran, D. H. Kim, N. H. Kim and J. H. Lee, *Small*, 2021, **17**, 2103826.

8 X. Wang, X. Liu, S. Wu, K. Liu, X. Meng, B. Li, J. Lai, L. Wang and S. Feng, *Nano Energy*, 2023, **109**, 108292.

9 L. Yang, C. Feng, C. Guan, L. Zhu and D. Xia, *Applied Surface Science*, 2023, **607**, 154885.

10 H. Sun, J. Sun, Y. Song, Y. Zhang, Y. Qiu, M. Sun, X. Tian, C. Li, Z. Lv and L. Zhang, *ACS Appl. Mater. Interfaces*, 2022, **14**, 22061–22070.

11 L. Xie, Q. Liu, X. He, Y. Luo, D. Zheng, S. Sun, A. Farouk, M. S. Hamdy, J. Liu, Q. Kong and X. Sun, *Chem. Commun.*, 2023, **59**, 10303–10306.

12 X. Fang, X. Wang, L. Ouyang, L. Zhang, S. Sun, Y. Liang, Y. Luo, D. Zheng, T. Kang, Q. Liu, F. Huo and X. Sun, *Molecules*, 2022, **27**, 7617.

13 Y. Liang, L. Zhang, Q. Liu, L. Ouyang, Y. Luo, D. Zheng, Y. Wang, S. Sun, X. Wang, J. Zhang, C. Xu and X. Sun, *Eur J Inorg Chem*, 2023, **26**, e202200657.

14 L. Wu, L. Yu, B. McElhenny, X. Xing, D. Luo, F. Zhang, J. Bao, S. Chen and Z. Ren, *Applied Catalysis B: Environmental*, 2021, **294**, 120256.

15 W. Li, S. Yang, X. Yan, L. Zhang, J. Wu, J. Wang, Q. Tang, F. Wang, C. Li, Y. Sun and H. Wu, *Applied Surface Science*, 2026, **715**, 164546.

16 Q. Liu, X. Fu, H. Li, J. Xing, W. Xiao, Y. Zong, G. Fu, J. Wang, Q. Cao, T. Ma, L. Wang and Z. Wu, *Chem. Sci.*, 2025, **16**, 13306–13315.

17 C. Kim, S. Lee, S. H. Kim, J. Park, S. Kim, S.-H. Kwon, J.-S. Bae, Y. S. Park and Y. Kim, *Nanomaterials*, 2021, **11**, 2989.

18 X. Chen, Y. Duan, H. Dou, W. Zhang and X. Wang, *Chemical Engineering Journal*, 2024, **499**, 155925.

19 X. She, C. Feng, D. Liu, Z. Fan, M. Yang and Y. Li, *International Journal of Hydrogen Energy*, 2024, **59**, 1297–1304.

20 Y. Liu, L. Wang, R. Hübner, J. Kresse, X. Zhang, M. Deconinick, Y. Vaynzof, I. M. Weidinger and A. Eychmüller, *Angewandte Chemie International Edition*, 2024, **63**, e202319239.

21 L. Xie, Q. Liu, X. He, Y. Luo, D. Zheng, S. Sun, A. Farouk, M. S. Hamdy, J. Liu, Q. Kong and X. Sun, *Chem. Commun.*, 2023, **59**, 10303–10306.

22 H. Li, X. Gao and G. Li, *Small*, 2023, **19**, 2304081.

23 H. Wang, L. Chen, L. Tan, X. Liu, Y. Wen, W. Hou and T. Zhan, *Journal of Colloid and Interface Science*, 2022, **613**, 349–358.

24 L. Yu, L. Wu, S. Song, B. McElhenny, F. Zhang, S. Chen and Z. Ren, *ACS Energy Lett.*, 2020, **5**, 2681–2689.